Quantitative analysis of surface enhanced Raman spectroscopy of Rhodamine 6G using a composite graphene and plasmonic Au nanoparticle substrate

Ryan Goul [a, *], Susobhan Das [b], Qingfeng Liu [a, **], Melisa Xin [a], Rongtao Lu [a], R. Hui [b], Judy Z. Wu [a, ***]

[a] Department of Physics and Astronomy, University of Kansas, Lawrence, KS, 66045, USA
[b] Department of Electrical Engineering & Computer Science, University of Kansas, Lawrence, KS, 66045, USA

ARTICLE INFO

ABSTRACT

A novel type of substrate for quantitative surface enhanced Raman spectroscopy (SERS) composed of chemical vapor deposition (CVD) graphene and in-situ fabricated rounded gold nanoparticles (AuNPs) was designed. SERS was measured on samples of different concentrations of Rhodamine 6G (R6G) on the AuNPs/graphene substrates using a low power 632.8 nm laser. Finite element simulations were carried out for a system of two gold hemiellipsoids under various conditions such as with R6G analyte covering the surface and with graphene underneath the nanoparticles. Graphene or R6G being present between the two nanoparticles caused a redshift in the plasmonic resonance frequency, and the graphene dampened the electric field of the surface. Regardless of the weakened electric field, the synergy of the AuNPs and graphene still enhanced the Raman signature of R6G to a greater extent than the nanoparticles or graphene alone could, which is attributed to the charge transferring mechanism effect of graphene on SERS. The lowest concentration of solid phase R6G deposited in this manner that could be detected was 8×10^{-7} M. Higher analyte concentrations and the characteristic peak intensities of the analyte showed a logarithmic relation as anticipated from the plasmonically enhanced Raman scattering.

© 2016 Elsevier Ltd. All rights reserved.

1. Introduction

Raman spectroscopy is a commonly used analysis tool, which can identify the composition of a given material or sample. However, basic Raman spectroscopy lacks the sensitivity that other spectroscopic detection methods have since out of the photons interacting with the analyte, as low as one in 10^8 photons will produce a Raman scattering event. That is why the push has been made to increase the sensitivity of Raman spectroscopy through various enhancement techniques such as resonance Raman spectroscopy (RRS) [1], tip enhanced Raman spectroscopy (TERS) [2,3], and surface enhanced Raman spectroscopy (SERS) [4]. Among others, SERS is particularly interesting since it allows an enhancement of several orders of magnitude of the Raman signal by modifying the surface upon which an analyte material is to be placed.

SERS substrates are theorized to utilize two mechanisms to increase the Raman scattering intensity [1]. The first is the electromagnetic mechanism, which typically comes from an analyte located near an enhanced electric field at the substrate surface created by the excitation of localized surface plasmons in the metal structures (nanoparticles in this experiment) present on the surface. This enhancement is possible since Raman scattering intensity is proportional to squared induced dipole moment, which is proportional to a product of the polarizability and incident electromagnetic field strength. Due to this, the Raman scattering intensity scales with local electric field strength at a rate of approximately E^4 [5]. The second is known as the chemical mechanism (or sometimes charge transfer mechanism), which involves the bonding of the analyte material to the substrate surface. This bonding increases the polarizability, and thereby Raman scattering intensity. Theoretically this is achieved by making the HOMO to LUMO

transition more easily attainable with intermediate energy states formed during bonding. Previous work has found the electric mechanism's enhancement factor of 10^8 (possibly up to 10^{10} under certain conditions) be dominant over the chemical mechanism's best enhancement factor which is approximately 10^2 [6].

Much of the recent research in SERS has been directed towards increasing the sensitivity of the substrates and enhancing their capabilities as biosensing devices by changing the dimensions/ shape of the nanoparticles or adding a layer of graphene to the substrate. Scarabelli et al. was able to demonstrate the enhancement effect caused by self-assembling nano-triangles (50–150 nm), which was achieved with an easily scalable seeding process, and appears promising for future applications in plasmonic device/ substrate fabrication [7]. Wei Fan et al. demonstrated the additional Raman enhancement that graphene can provide in a substrate with graphene oxide and Ag octahedral nanoparticles. Additionally, they concluded that since the reduced graphene oxide samples showed weaker SERS enhancement, that the charge transfer between the oxygen functional groups was the primary enhancement mechanism provided by the graphene oxide [8]. Xuanhua Li et al. were able to fabricate a novel surface that uses graphene as a nanospacer between a bulk Ag layer and Ag nanospheres on top of the graphene, which gave them massively enhanced Raman signal due to what they described as extra coupling modes between the bulk metal and the nanoparticles as opposed to only the nanoparticles coupling to one another [9].

Previous work done by Lu et al. in our lab [10] employing Rhodamine 6G (R6G) as a test molecule showed a unique synergy in a SERS substrate that used a combination of gold nanoparticles (AuNP) and graphene. The AuNPs on the substrate most closely resemble hemispheres/hemiellipsoids in that they have a flat bottom (contacting the grapheme layer) and are round on the air/Au interface side. Enhanced Raman scattering is supplied by the AuNPs through the electromagnetic mechanism by providing a strong local electric field while the graphene is theorized to provide enhancement through the charge transfer mechanism due to its resonance frequency being in the far infrared to THz region and its low electron density [11]. However, when the graphene and AuNP were combined, the enhancement was found to be greater than the enhancement that the nanoparticles or graphene alone could provide.

Advantageous characteristics of this substrate are not limited to the enhancement of Raman scattering. Graphene, from chemical vapor deposition (CVD), and the AuNP, deposited via *in situ* electron beam deposition at moderately elevated temperatures, provide a uniform surface upon which the analyte material may attach [11–13]. This substrate would allow more consistent results if this type of surface were to be used on a large scale in the medical industry for example. For AuNPs the resonance for the surface plasmons is located at approximately 600 nm with some variance depending on the shape and dimensions of the nanoparticles [10,14]. This resonance lies within the visible region, perfect for Raman spectroscopy, which commonly uses a red laser (632.8 nm) for analysis of more easily damaged analytes such as biomolecules.

With graphene-based SERS substrates, the adsorbed organic and biomolecules have an interaction with the carbon atoms more easily than they do with metal molecules. Such an interaction is even stronger when using an aromatic molecule, because the hexagonal honeycomb shaped pattern formed by the sp2 carbon atoms of graphene allows for a stronger interaction through π-bond interactions with the remaining 2pz π orbital [11]. Furthermore, graphene has the ability to quench fluorescence from the attached molecules [15]. Quenching is invaluable in the analysis of fluorescent molecules, such as R6G, where the fluorescent background would dominate and make Raman detection of the molecule more difficult.

Other similar substrates have been studied by various groups recently. Tiangcheng Gong et al. [16] experimented with silver nanoparticles (AgNP) on graphene (and graphene on top of AgNP) in order to find a more cost-efficient way to produce AgNP based SERS substrates. They used a recent technique known as the "vector decomposition method" to separately analyze how strain and n-doping affected shifts in the G and 2D peaks of graphene in this hybrid structure. Longyun Zhao et al. [17] similarly produced a hybrid AuNP/graphene substrate, but using a colloidal solution with the purpose using SERS to detect Pb^{2+} ions. Another interesting step in the direction of uniformity in graphene/AuNP SERS substrates was achieved by Shicai Xu et al. [18] when their group used AuNP arrays with a layer of graphene covering the top of the array. Similar to our own substrate, they used e-beam evaporation for Au deposition, but used masks and chemical etching to obtain their desired morphology while we used in-situ heating during the deposition.

This study seeks to further the work of Lu et al. [10] firstly by quantifying the optical and electromagnetic properties of the substrate and secondly, by analyzing the sensitivity limits of this specific graphene/AuNP SERS substrate. In the following, we report our results.

2. Experimental methods

Graphene samples were prepared using the CVD method on Cu foils in a furnace with a combination of H_2 and CH_4 at ~1000 °C [19,20]. Poly(methyl methacrylate) (PMMA) was then spun on top of the graphene/Cu for graphene transfer. More details of the transfer procedure can be found elsewhere [19]. Briefly, Cu/graphene/PMMA strips were then floated (PMMA side up) in Cu etchant to remove all Cu from the strips. Afterwards, the graphene/ PMMA was rinsed multiple times with deionized water, transferred onto the target substrate (doped Si with 90 nm SiO_2 on the top layer), and heated on a hotplate at 80 °C for 1 h in air to improve the interface between graphene and the SiO_2. In order to remove the PMMA, the sample was submerged in acetone and isopropanol, and then dried with N_2 gas. Post-annealing in a furnace at 450 °C under a flow of mixed Ar and H_2 (500 sccm each) was employed to remove the polymer and chemical residues on graphene [19,20].

The integrity of the graphene was checked via comparison of the Raman peak intensities for the D-peak (~1355 cm^{-1}), which arises from defects in the graphene, and the G peak (~1585 cm^{-1}). On most samples used in this experiment, the D-peak has a negligible intensity, confirming the graphene's high quality (Fig. S1). In addition, the intensity ratio between the 2D and G peaks is around 1.2 or higher, indicating the graphene is single-layered. Plasmonic AuNPs were evaporated *in situ* in an e-beam deposition chamber at vacuum better than 10^{-6} Torr. During the deposition, the sample temperature was maintained at ~300 °C, which is close to the Au/ graphene eutectic temperature for the AuNPs to form during the deposition. The nominal thickness of the Au film was selected to be 12 nm for optimal plasmonic effect in SERS study [10]. After deposition of AuNPs, the peak intensities of graphene increase while the relative intensity of 2D to G peak ratio is suppressed, as shown in Fig. S1 [10]. The AuNP morphology was examined using an LEO 1550 field-emission scanning electron microscopy (SEM). Previous papers published by our group have focused determining the optimal preparation conditions for the layer of AuNPs. In order to obtain more rounded nanoparticles, a high temperature is required, but the temperature cannot be too high or else there is a risk that the graphene could be damaged. Therefore an optimal temperature (300 °C) was found in order to create the most effective SERS nanoparticles of this type with a small interparticle

gap distance and simultaneously develop a better interface between the AuNPs and graphene [10]. An additional Raman scan was performed on the substrate after the deposition of AuNPs to confirm that the graphene's quality persisted through the process (Fig. S1).

Samples with different concentrations of R6G in the range of 5×10^{-5} M to 4×10^{-7} M were prepared combining solid phase Sigma Life Science R6G and deionized water to make the highest concentration solution. Lower concentration samples were made by diluting the highest concentration solution of R6G. To place the R6G onto the substrates, a single droplet of a given concentration was cast onto the surface. The droplet (~3—4 mm in diameter) was then dried in atmosphere inside a dish placed on a hotplate at 70 °C. For Raman spectroscopy, the laser beam spot of sub-millimeter was reasonably small allowing multiple scan locations in the center of each drop. Additionally, a low intensity and small integration time of 3 s were used and each spectrum recorded was the result of an average of 25 measurements.

To analyze the effects of graphene and R6G with different levels of concentration, a simulation with COMSOL Multiphysics based on finite element method (FEM) was performed with the excitation optical field polarized parallel to the graphene surface [21,22]. The shape of AuNPs were assumed to be hemiellipsoid with the average dimensions of 20 nm in height and 40 nm in diameter, and the gap between adjacent AuNPs was 9 nm. These values are within half of a standard deviation of the average nanoparticle dimensions, which are obtained by using the ImageJ software package to analyze SEM images of the substrates [10]. The AuNps were placed on top of silica substrate with a 0.34 nm thick single layer graphene between them, as shown in Fig. 1a. A layer of R6G with 2 nm thickness was placed on top of graphene surrounding the AuNps. The impact of R6G concentration change was modeled by varying the refractive index of the R6G layer in the simulation.

3. Discussion of results

Both the graphene and the AuNP play a role in the enhancement of the Raman scattering. The AuNP through their plasmonic electric field (Fig. 1d), and the graphene is believed to provide enhancement from a charge transferring mechanism [11]. However, for the electric field enhancement, the most important area of the substrate is in between AuNPs. A lone AuNP will still contribute an electric field to its surroundings, but two or more AuNPs that are near each other will produce a much stronger field on the substrate surface between them [10]. The SEM image in Fig. 1e shows the spacing of this particular substrate to be between 5 and 30 nm. Hemispheres are one of the most effective plasmonic nanoparticle geometries in terms of enhancing light scattering. There is also an optimum diameter for these hemispheres wherein the Ohmic loss (which scales with volume) is minimized, and the scattering (which scales with volume squared) is maximized. Our nanoparticles were approximately 40 nm in diameter on average based on data from our past experiments [10] (Fig. 1e), which is very near to this optimum dimension [23]. The simulated cross sectional electric field distributions in two different planes (Fig. 1f) (the top figure shows the xz plane at y = 0, and the bottom figure shows xy plane at z = 0) indicate that the electric field is significantly enhanced between each pair of AuNPs and near their surfaces. This incident field travels orthogonally towards the surface on the nanoparticles side in the simulation.

Typically, the R6G (which has many ring groups in its molecular structure) is thought to bond through π bonding with the rings of the graphene. That means that typically in our substrate, we would expect the Raman signal to come primarily from R6G molecules bonded to the graphene between the AuNP where the electric field

enhancement is strongest (Fig. 1b and c). As was mentioned previously, the R6G was placed on the substrate by drying droplets of various concentrations onto it (Fig. 2a). This method is effective at producing the appropriate concentration of R6G as can be seen from the increase in fluorescence intensity as the fluorescent dye concentration increases (Fig. 2b) [24]. However, at higher concentrations (in the 10^{-4} M and above range) the R6G Raman signal will become dampened, but this will be analyzed later in the discussion of the Raman peak intensity analysis. This is likely due to excess R6G bunching up on top of each other as drying occurs, meaning that any signal from those molecules would receive less enhancement from the substrate.

In order to confirm the plasmonically enhanced electric field of the AuNP, optical transmission spectra were taken in visible range at different R6G concentrations as shown in Fig. 3a. The transmission spectrum of a single layer graphene alone is nearly flat, which is expected since each layer of the graphene sheet absorbs ~2.3% of the incident white light. The AuNP/graphene spectra show a plasmonic transmission dip (absorption peak) between 525 nm and 625 nm with a minimum transmission of approximately 50%, illustrating the localized surface plasmonic resonance (LSPR) of AuNPs. This observation is consistent with our previous report on similar substrates and the resonance frequency was found to vary in proximity of 600 nm depending on the dimension and spacing of the AuNP's [10]. Also included in Fig. 3a are two transmission spectra measured on AuNP/graphene with 10 μM and 50 μM R6G, respectively. These spectra were taken with the incident light shining through the center of each droplet of dried R6G on the substrate. However, due to the large size of the light beam (2—3 mm in diameter), a small fraction of the light may have shined on the outside ring of the droplets where aggregate R6G dried. A red shift of the LSPR resonance can be observed with the adding of R6G, and this red shift is increased with the increase of R6G concentration.

To understand the effect of R6G concentration on the LSPR resonance, numerical finite element simulations of the transmittance were carried out for five different configurations including AuNP only, AuNP/graphene without R6G, and AuNP/graphene with three different concentrations of R6G on the substrate. The calculated transmittances within the wavelength range between 400 nm and 800 nm are shown in Fig. 3b. To reiterate, this was simulated using Adding graphene underneath AuNPs, the plasmonic resonance shifted to a longer wavelength and the spectrum became broader in comparison to that without graphene. After adding R6G on the AuAP/graphene, the LSPR resonance is further damped and the resonance wavelength is red shifted depending on the concentration of R6G. The red shift of plasmonic resonance at higher concentration of R6G is attributed to the increased permittivity of the R6G layer, which modifies the plasmonic resonance condition. Meanwhile, with higher concentration of R6G, the loss factor also increases, contributing to the decrease of Q-value and the broadening of the resonance transmission dip as depicted in Fig. 3b.

Although R6G covers only portions of the areas in a random manner between AuNPs as illustrated in Fig. 1b and c, we used a 2 nm thick uniform layer of R6G in the simulation with appropriate permittivity to account for the concentration level of the R6G. Considering the refractive index of R6G of $n = 2.3$ (± 0.05) $+ i0.03$ (± 0.02) [25,26] at the 100% concentration level and $n = 1$ (refractive index of air) at 0% concentration, the impact of R6G is incorporated in the simulation by linearly interpolating the refractive index between 0% and 100% concentrations. The permittivity and loss factor of R6G surrounding AuNP linearly increase as the concentration increases. Theoretically, the strength of plasmonic resonance is proportional to $1/(\varepsilon_m + M\varepsilon_b)$ where ε_m and ε_b are the permittivities of the metal and the surrounding dielectric materials, respectively.
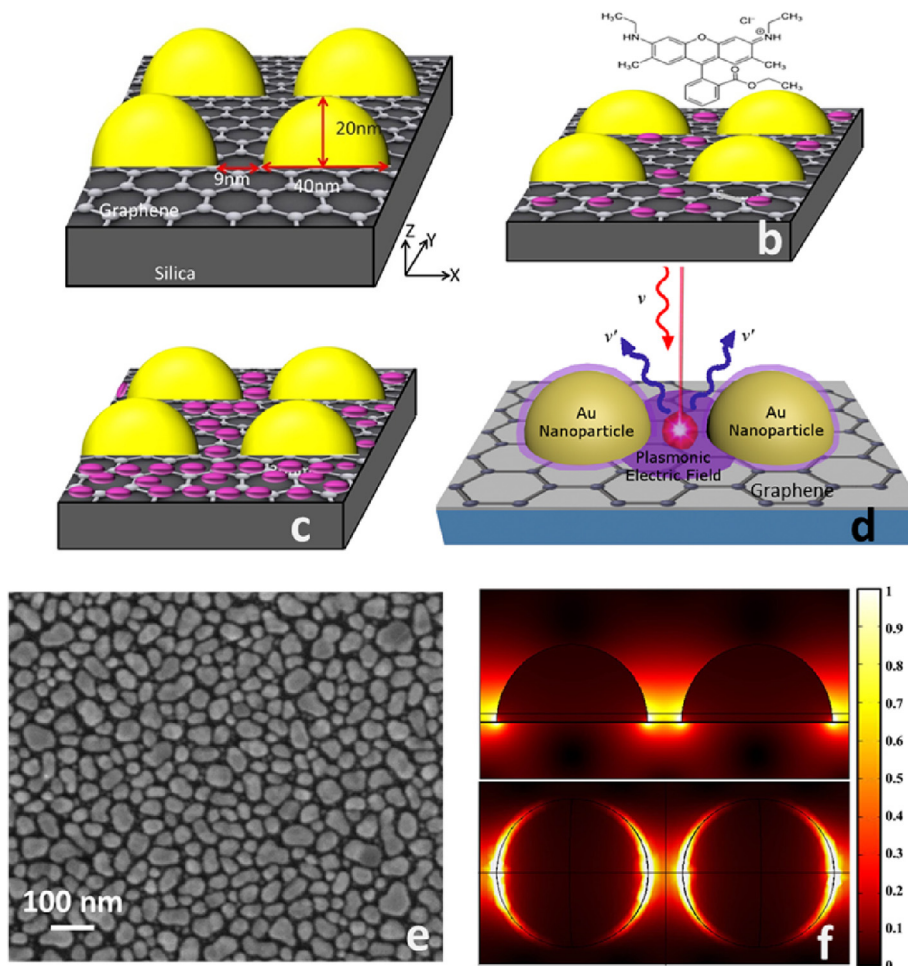
Fig. 1. (a) Diagram of AuNPs on SiO$_2$/Si substrate surface. (b) R6G molecules (depicted as purple spheroids) partially covering the substrate. (c) R6G molecules fully covering the substrate. (d) Diagram of plasmonic AuNP enhancing Raman scattering with their electric field. (e) SEM image of AuNP on graphene and silicon. Another enlarged SEM image of this substrate type is available in the supporting information Fig. S2 (f) Electric field distribution normalized to the value of the incident electric field of the two AuNP's from the side xz plane (top) and from above looking at the xy plane (bottom). Note: Fig. 1a—d are not to scale. (A colour version of this figure can be viewed online.)
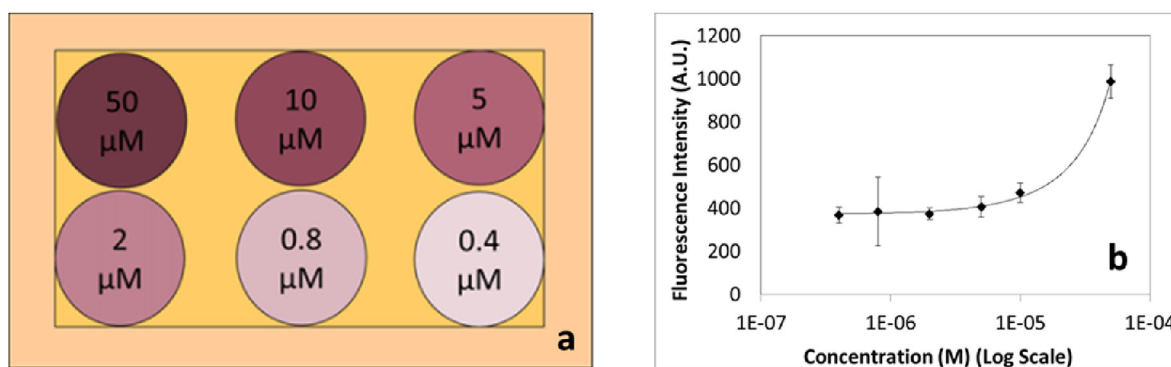
Fig. 2. (a) R6G droplet deposition method on top of graphene (smaller rectangle) and AuNP (everywhere on substrate). (b) Fluorescence intensities for droplets with different concentrations of R6G on a AuNP/graphene/Si substrate, concentration is shown on a logarithmic scale. (A colour version of this figure can be viewed online.)

M is a structural-dependent factor, which varies with the geometry but is typically of the order of one. Therefore, the conditions for plasmonic resonance can be met when the metallic permittivity (which is more negative at longer wavelengths) is nearly opposite to the permittivity of the surrounding medium. As the permittivity of R6G surrounding the AuNP increases with increasing

concentration, a redshift in the plasmonic resonance is introduced.

Fig. 3c shows the normalized x-polarized electric field (x-and y-axes are in the plane of the substrate, while z-axis is perpendicular to the substrate and the electric field normalized to the strength of the incident field) distribution in the gap region between two AuNPs. As the R6G concentration increases, the electric field near
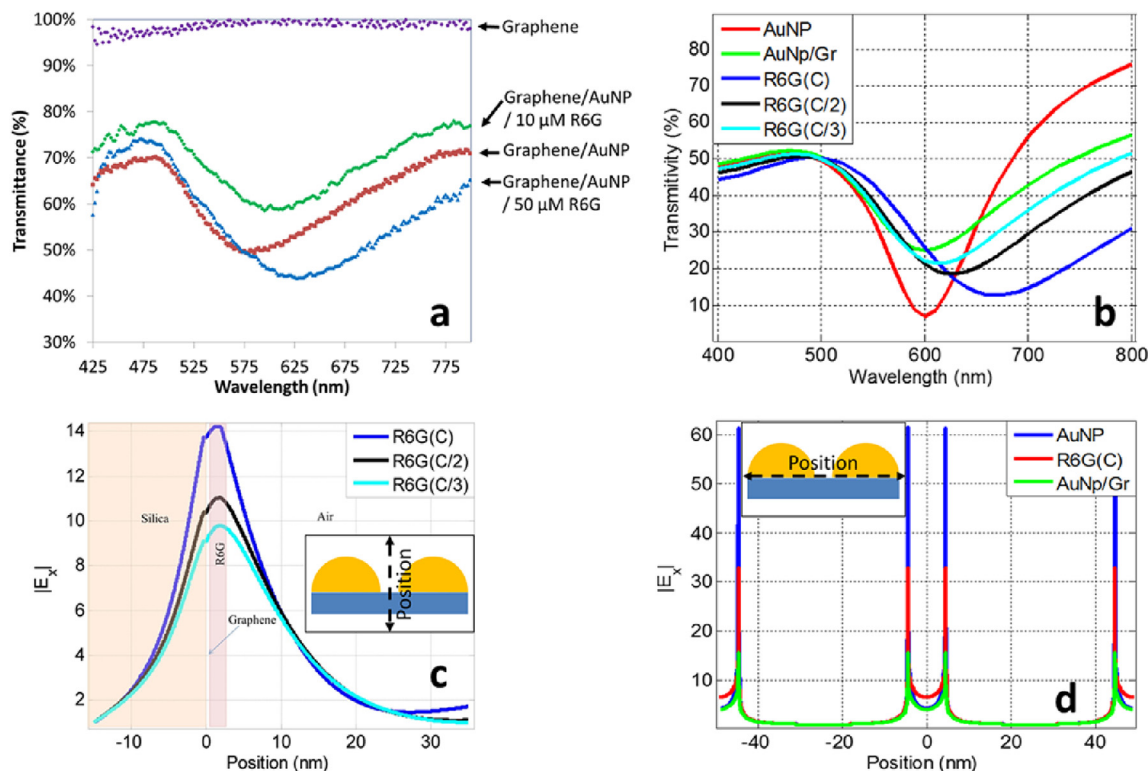
Fig. 3. (a) Typical transmission spectra of multiple materials on fused silica, and of different concentrations of R6G on top of these materials. (b) Simulation results of typical transmitivity over the wavelength range of 400 nm–800 nm is shown for different conditions. R6G curves represent R6G on top of the graphene/AuNP substrate, while the C/2 and C/3 curves represent R6G at one-half and one-third of the maximum concentration C. The red and green curves represent a substrate with only AuNP and one with AuNP and graphene respectively. (c) Normalized Electric field distribution in the gap between two AuNP's for different concentration levels of R6G, position is in the z-direction. (d) Normalized electric field distribution about the bottom of two nano-particles under different conditions, position is in the x-direction with 0 being the center between the two AuNPs (larger, separate results for each simulation are available in the supporting information Fig. S3). (A colour version of this figure can be viewed online.)

AuNP is enhanced which overlaps the region covered by R6G. The x-polarized electric field, normalized to the incident field strength as well, on the graphene surface is shown in Fig. 3d. For the three interface structures, the highest electric field is obtained with the AuNP only, and the lowest electric field intensity occurs when the graphene layer is added on substrate but without R6G. This is due to the conductive graphene dissipating the near field on and around the AuNPs and thus resulting in the dampening of the plasmonic resonance [10]. When insulating R6G is introduced onto the graphene between the AuNPs, the plasmonic field intensity is increased in relation to the amount of R6G between the particles, and the substrate experiences greater plasmonic field intensity with higher concentrations of R6G.

With an understanding of the plasmonic effect on the SERS signals in the presence of R6G molecules, we may now look to see to what extent the electric field enhances Raman signal. The Raman signature peaks of R6G are clearly visible at every tested concentration (Fig. 4), which is in contrast to negligible signals on other substrates such as basic Si/SiO_2 or Si/SiO_2/graphene [10]. Note that the spectrum's intensity at 8×10^{-7} M R6G concentration has been increased by a factor of five in order to be comparable to the spectra measured at larger concentrations. One lower level of concentration than the minimum in Fig. 4 (4×10^{-7} M) was also tested, but no Raman signal could be detected. This implies that the sensitivity limit of this AuNP/graphene substrate is approximately 8×10^{-7} M or possibly slightly lower. The Raman signals are much stronger with well-defined peaks at higher R6G concentration, which may be attributed to the combined effect of high Raman signals proportional to the concentration of the R6G molecules, and the
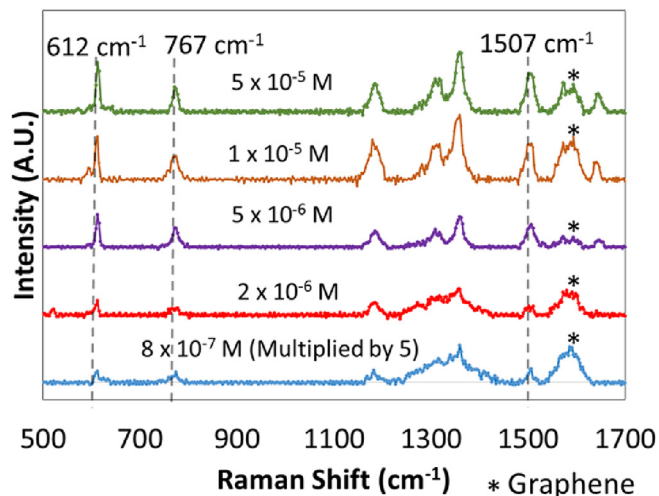
Fig. 4. Raman spectra taken for five different concentrations (in moles per liter) on the Si/graphene/AuNP substrate. Spectra are offset from one another, and share a common scale with the exception of the 8×10^{-7} M spectrum, which was scaled up by a factor of 5 to make it easier to compare with the other spectra. The G-mode of graphene at 1590 cm^{-1} is marked with a *, while the dotted lines denote the 612 cm^{-1}, 767 cm^{-1}, and 1507 cm^{-1} peaks in the R6G Raman spectra. (A colour version of this figure can be viewed online.)

enhanced SERS signals due to higher R6G concentration as shown in Fig. 4. Further analysis was carried out using a substrate with graphene on top of the AuNPs and taking spectra of both substrate
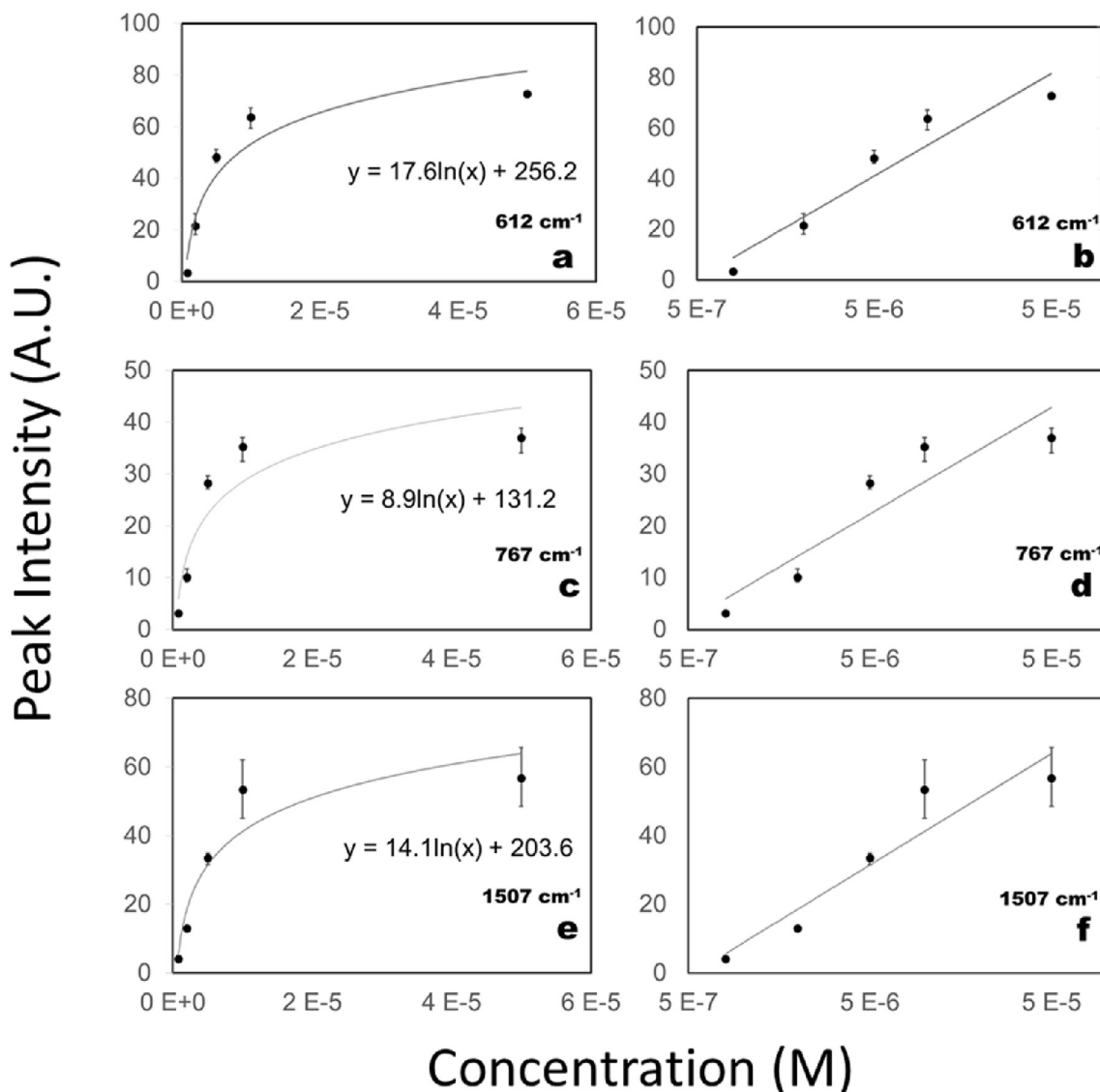
Fig. 5. (**a–f**): Shows the intensities of the Raman peaks of R6G at 612 cm^{-1} (a, b), 767 cm^{-1} (c, d), and 1507 cm^{-1} (e, f) plotted against the concentration of R6G. The left side (a, c, e) was plotted using a linear scale on the x-axis, while the right side (b, d, f) was plotted using a logarithmic scale.

configurations using a higher energy 488 nm laser. Even with these modifications, we were unable to observe characteristic R6G peaks at a concentration of 10^{-7} M. The details and figures concerning these extra experiments are located in the supporting information.

Looking at the details of several papers dealing with SERS and R6G, the earlier mentioned paper by Shicai Xu et al. made use of Au nanosphere arrays with graphene blanketing them and an excitation wavelength of 532 nm in order to attain a sensitivity of 10^{-11} M [18]. Feng et al. used n-doped graphene in order to attain Raman signals of Rhodamine B (RhB) at 10^{-11} M and R6G at 10^{-8} M (though based on their results it appears as if they would be able find even lower concentrations of R6G on their substrates) [27]. That group also found that their 514.5 nm (2.41 eV) laser gave the highest Raman intensity (relative to the graphene G peak intensity) for RhB. Further investigation led them to conclude that this was due in large part to matching of the HOMO/LUMO gap of the analyte to the laser excitation energy. Due to these results it leads us to believe that a 514 or 532 nm laser would give us added sensitivity by resonating with this energy gap. Unfortunately we were unable to

acquire access to a Raman system with either of those wavelengths during the course of this experiment.

Further analysis was done on the height of several peaks of the R6G spectrum. The peaks at 612 cm^{-1}, 767 cm^{-1}, and 1507 cm^{-1} were chosen because they are sufficiently distinct above the initial background, and are far enough away from the characteristic graphene and Si peaks that they can be confirmed to originate from the R6G. Fig. 5a, c, and e show the logarithmic relation between the Raman peak intensity and the concentration of R6G, and when viewing Fig. 5 b, d, and f with a logarithmic scale for the concentration axis, it is clear that their relationship is logarithmic. This relation has been noted in other studies involving nanoparticles and SERS using a variety of analyte molecules/elements [28–31].

However, the 5 × 10^{-5} M data point does not seem to fit the trend as well as we would like. Based on the resonance peak shift in Fig. 3, this is likely due to the high R6G concentration influencing the amount of resonance scattering occurring and due to excess R6G preventing the short range electric field from reaching and enhancing the topmost R6G molecules.

4. Conclusion

In conclusion, through a quantitative study of SERS signatures of R6G molecules attached to plasmonic AuNPs/graphene/SiO$_2$ substrates, we have demonstrated the sensitivity limit of 8×10^{-7} M using solid phase R6G attached (dried) to the SERS substrate. This limit could likely be improved if our group had access to a ~514 nm or ~532 nm laser with an energy level closer to the HOMO/LUMO gap of R6G. An in-depth simulation of the evanescent field around the plasmonic AuNPs has revealed interactions between the R6G molecules with the plasmonic AuNPs/graphene substrates and the information is important to further optimization of the SERS for higher sensitivity. What remains to be determined is how exactly the AuNP's and graphene are interacting at a quantitative level through charge transfer in order to produce this effect.

Acknowledgements

Appendix A. Supplementary data

Supplementary data related to this article can be found at http://dx.doi.org/10.1016/j.carbon.2016.10.019.

References

[1] G.D. Ewen Smith, Modern Raman Spectroscopy - a Practical Approach, John Wiley & Sons, Ltd, West Sussex, England, 2005.

[2] Matthew D. Sonntag, Jordan M. Klingsporn, Luis K. Garibay, John M. Roberts, Jon A. Dieringer, Karl A. Scheidt, et al., Single-molecule tip-enhanced Raman spectroscopy, J. Phys. Chem. C 116 (1) (2012) 478–483.

[3] R. Zhang, Y. Zhang, Z.C. Dong, S. Jiang, C. Zhang, L.G. Chen, et al., Chemical mapping of a single molecule by plasmon-enhanced Raman scattering, Nature 498 (2013) 82–86.

[4] Dana Cialla, Anne März, René Böhme, Frank Theil, Karina Weber, Michael Schmitt, et al., Surface-enhanced Raman spectroscopy (SERS): progress and trends, Anal. Bioanal. Chem. 403 (1) (2012) 27–54.

[5] Paul L. Stiles, Jon A. Dieringer, Nilam C. Shah, Richard P. Van Duyne, Surface-enhanced Raman spectroscopy, Annu. Rev. Anal. Chem. 1 (2008) 601–626.

[6] Sebastian Schlücker, Surface-enhanced Raman spectroscopy: concepts and chemical applications, Angew. Chem. 53 (19) (2014) 4756–4795.

[7] Leonardo Scarabelli, Marc Coronado-Puchau, Juan J. Giner-Casares, Judith Langer, Luis M. Liz-Marza, Monodisperse gold Nanotriangles: size control, large-scale self-assembly, and performance in surface-enhanced Raman scattering, ACS Nano 8 (6) (2014) 5833–5842.

[8] Wei Fan, Yih Hong Lee, Srikanth Pedireddy, Qi Zhang, Tianxi Liu, Xing Yi Ling, Graphene oxide and shape-controlled silver nanoparticle hybrids for ultrasensitive single-particle surface-enhanced Raman scattering (SERS) sensing, Nanoscale 6 (2014) 4843–4851.

[9] Xuanhua Li, Wallace C.H. Choy, Xingang Ren, Di Zhang, Haifei Lu, Highly intensified surface enhanced Raman scattering by using monolayer graphene as the nanospacer of metal film−metal nanoparticle coupling system, Adv. Funct. Mater. 24 (21) (2014) 3114–3122.

[10] Rongtao Lu, A. Konzelmann, Feng Xu, Youpin Gong, Jianwei Liu, Qingfeng Liu, et al., High sensitivity surface enhanced Raman spectroscopy of R6G on in situ fabricated Au nanoparticle/graphene plasmonic substrates, Carbon 86 (2015) 78–85.

[11] Weigao Xu, Nannan Mao, Jin Zhang, Graphene: a platform for surface-enhanced Raman spectroscopy, Small 9 (8) (2013) 1206–1224.

[12] Liming Xie, Xi Ling, Yuan Fang, Hua Xu, Haoli Zhang, Jing Kong, et al., Can graphene be used as a substrate for Raman enhancement? Nano Lett. 10 (2) (2010) 553–561.

[13] Xi Ling, Weigao Xu, Jiaqi Xiao, Mildred S. Dresselhaus, Jing Kong, Hongxing Xu, et al., Surface enhanced Raman spectroscopy on a flat graphene surface, Natl. Acad. Sci. 109 (24) (2012) 9281–9286.

[14] Yingying Wang, Zhenhua Ni, Hailong Hu, Yufeng Hao, Choun Pei Wong, Ting Yu, et al., Gold on graphene as a substrate for surface enhanced Raman scattering study, Appl. Phys. Lett. 97 (2010), 163111–1 − 163111-4.

[15] Liming Xie, XLing, Yuan Fang, Jin Zhang, and Zhongfan Liu Graphene as a substrate to suppress fluorescence in resonance Raman spectroscopy J. Am. Chem. Soc. 131(29): 9890−9891.

[16] Tiancheng Gong, Jie Zhang, Yong Zhu, Xinyu Wang, Xiaolei Zhang, Jing Zhang, Optical properties and surface-enhanced Raman scattering of hybrid structures with Ag nanoparticles and graphene, Carbon 102 (2016) 245−254.

[17] Longyun Zhao, Wei Gu, Cuiling Zhang, Xinhao Shi, Yuezhong Xian, In situ regulation nanoarchitecture of Au nanoparticles/reduced graphene oxide colloid for sensitive and selective SERS detection of lead ions, J. Colloid Interface Sci. 465 (2016) 279−285.

[18] Shicai Xu, Shouzhen Jiang, Jihua Wang, Jie Wei, Weiwei Yue, Yong Ma, Graphene isolated Au nanoparticle arrays with high reproducibility for high-performance surface-enhanced Raman scattering, Sensors Actuators B 222 (2016).

[19] Qingfeng Liu, Youpin Gong, Jamie Samantha Wilt, Ridwan Sakidja, Judy Wu, Synchronous growth of AB-stacked bilayer graphene on Cu by simply controlling hydrogen pressure in CVD process, Carbon 93 (2015) 199−206.

[20] Qingfeng Liu, Youpin Gong, Ti Wang, Wai-lun Chan, Judy Wu, Metal-catalyst-free and controllable synthesis of monolayer, bilayer and few-layer graphene on silicon dioxide by chemical vapor deposition, Carbon 96 (2016) 203−211.

[21] Sergei Tretyakov, Analytical Modeling in Applied Electromagnetics, Artech House, Norwood MA, 2000.

[22] COMSOL Multiphysics - RF Module, 2016.

[23] Harry A. Atwater, Albert Polman, Plasmonics for improved photovoltaic devices, Nat. Mater. 9 (2010) 205−213.

[24] Florian M. Zehentbauer, C. Moretto, Ryan Stephen, Thangavel Thevar, John R. Gilchrist, Dubravka Pokrajac, et al., Fluorescence spectroscopy of Rhodamine 6G: concentration and solvent effects, Elsevier 121 (2014) 147−151.

[25] Ali Qassim Abdullah, Surface and volume energy loss, optical conductivity of Rhodamine 6G dye (R6G), Chem. Mater. Res. 3 (10) (2013).

[26] Ali Qassim Abdullah, Alaa Yassin AL-Ahmad, Hadi Ziara AL-Sawaad, A study of some optical properties of PHMNP thin film, Walailak J. Sci. Tech. 10 (2) (2013) 159−168.

[27] Simin Feng, Maria Cristina dos Santos, Bruno R. Carvalho, Ruitao Lv, Qing Li, Kazunori Fujisawa, et al., Ultrasensitive molecular sensor using N-doped graphene through enhanced Raman scattering, Sci. Adv. 2 (2016).

[28] Lateef U. Syed, Luxi Zhang Swisher, Hannah Huff, Caitlin Rochford, Fengli Wang, Judy Wu Jianwei Liu, Mark Richter, Sivasai Balivada, Deryl Troyer, Jun Li, Luminol-labeled gold nanoparticles for ultrasensitive chemiluminescence-based chemical analyses, Analyst 138 (2013) 5600−5609.

[29] Ming Li, Jianming Zhang, Savan Suri, Letha J. Sooter, Dongling Ma, Nianqiang Wu, Detection of adenosine triphosphate with an aptamer biosensor based on surface-enhanced Raman scattering, Anal. Chem. 84 (6) (2012) 2837−2842.

[30] W.S. Shi1, X.T. Wang, G.W. She, L.X. Mu, S.T. Lee, High-performance surface-enhanced Raman scattering sensors based on Ag nanoparticles-coated Si nanowire arrays for quantitative detection of pesticides, Appl. Phys. Lett. 96 (2010) 0531041−0531043.

[31] Yu Shi, Houyu Wang, Xiangxu Jiang, Bin Sun, Bin Song, Yuanyuan Su, et al., Ultrasensitive, specific, recyclable, and reproducible detection of lead ions in real systems through a polyadenine-assisted, surface-enhanced Raman scattering silicon chip, Anal. Chem. 88 (7) (2016) 3723−3729.